among the drugs used in the current analysis. For example, the topoisomerase I group is comprised solely of camptothecin derivatives, and we do not yet know whether the network will recognize chemically different subclasses of topoisomerase I agents when and if they are identified. Finally, mechanisms operating in the assay may not always be the most prominent ones in vivo or in other cell culture systems.

As often happens, some of the most intriguing clues may come from the data that do not fit. For example, the network with three hidden layer PEs classified mitomycin and porfiromycin as antimitotics instead of alkylating agents. (When five or more hidden layer PEs were used, the classifications were correct.) Interestingly, these compounds react in the minor groove of DNA, whereas all of the other alkylators in the data set react in the major groove. It will be important, therefore, to test other types of minor groove binders, such as tomaymycin, the anthramycins, and the pyrrolo-1,4-benzodiazepines. The classification network thus appears to be a good source of clues as to the fine structure of mechanistic categories, and sometimes those clues come from a comparison of optimal and nonoptimal networks.

We are currently using neural networks in the prospective analysis of new compounds tested by the NCI drug screening program. It appears that neural computing, when combined with other statistical techniques for pattern recognition and decision making, can play a productive role in the development of new agents for the treatment of such diseases as cancer and acquired immunodeficiency syndrome (AIDS).

REFERENCES AND NOTES

1. M. R. Boyd, *Princ. Pract. Oncol. Updates* **3**, 1 (1989).
2. K. D. Paull *et al.*, *J. Natl. Cancer Inst.* **81**, 1088 (1989).
3. R. Bai *et al.*, *J. Biol. Chem.* **266**, 15882 (1991); K. D. Paull *et al.*, *Cancer Res.* **52**, 3892 (1992); H. N. Jayaram *et al.*, *Biochem. Biophys. Res. Commun.* **186**, 1600 (1992); K. D. Paull, E. Hamel, L. Malspeis, in *Cancer Chemotherapeutic Agents*, W. E. Foye, Ed. (American Chemical Society, Washington, DC, in press).
4. T. Khanna, *Foundations of Neural Networks* (Addison-Wesley, New York, 1991); H. H. Szu, *Telemat. Inform.* **7**, 403 (1990).
5. J. Dayhoff, *Neural Network Architectures* (van Nostrand Reinhold, New York, 1990).
6. B. Demeler and G. Zhou, *Nucleic Acids Res.* **19**, 1593 (1991); A. V. Lukashin *et al.*, *J. Biomol. Struct. Dyn.* **6**, 1123 (1989); S. Brunak, J. Engelbrecht, S. Knudsen, *Nucleic Acids Res.* **18**, 4797 (1990); M. C. O'Neill, *ibid.* **19**, 313 (1991).
7. L. H. Holley and M. Karplus, *Proc. Natl. Acad. Sci. U.S.A.* **86**, 152 (1989); D. G. Kneller, F. E. Cohen, R. Langridge, *J. Mol. Biol.* **214**, 171 (1990); M. J. McGregor, T. P. Flores, M. J. E. Sternberg, *Protein Eng.* **2**, 521 (1989).
8. G. L. Wied *et al.*, *Anal. Quant. Cytol. Histol.* **12**, 417 (1990); W. H. Wolberg and O. L. Mangasarian, *ibid.*, p. 314; H. E. Dytch and G. L. Wied, *ibid.*, p. 379.
9. J. M. Boone, V. G. Sigillito, G. S. Shaber, *Med. Phys.* **17**, 234 (1990); J. S. DaPonte and P. Sherman, *Comput. Med. Imag. Graph.* **15**, 3 (1991).
10. M.-M. Mesulam, *Neurol. Prog.* **28**, 597 (1990).
11. S. Kurogi, *Biol. Cybern.* **64**, 243 (1991).
12. N. H. I. Mann and M. D. Brown, *Orthop. Clin. North Am.* **22**, 303 (1991).
13. N. Asada *et al.*, *Radiology* **177**, 857 (1990).
14. D. E. Rumelhart, G. E. Hinton, R. J. Williams, *Nature* **323**, 533 (1986).
15. Insofar as possible, construction of the database was kept independent of prior knowledge of results in the screen. However, screen results were used in a number of cases for the limited purpose of deciding which dose-range vector for a given drug captured the dynamic range of activity. Halichondrin B was initially predicted on the basis of COMPARE analysis of screen results to be an antitubulin agent, and that was later verified experimentally.
16. K. D. Paull *et al.*, *Proc. Am. Assoc. Cancer Res.* **29**, 488 (1988); M. C. Alley *et al.*, *Cancer Res.* **48**, 589 (1988); D. Scudiero *et al.*, *ibid.*, p. 4827; R. H. Shoemaker *et al.*, in *Prediction of Response to Cancer Chemotherapy*, T. Hall, Ed. (Liss, New York, 1988), pp. 265–286; A. Monks *et al.*, *J. Natl. Cancer Inst.* **83**, 757 (1991).
17. Network type: feed-forward, back-propagation; control strategy: normal cumulative delta learning with epoch size 30 and random presentation of input vectors during training. Initial learning coefficients and momentum: 0.3 and 0.45 for the hidden layer and 0.15 and 0.4 for the output layer (all four values decreased by a factor of 2 after 10,000 presentations). The extent of training was 15,000 presentations. (This was determined in preliminary experiments to fall within a broad optimal range with respect to the root-mean-square error of prediction in the ten test sets. This approach to cross-validation has general application.) Classification rule: plurality wins. For each pair of training and test sets, the network was trained and then tested seven times from seven different initial random numbers. The resulting output values were then averaged, a procedure that decreased considerably the number wrongly predicted (for example, from a mean of 15.4 to 12 in the case of seven hidden layer elements).
18. Statistical Analysis System/Statistics (*SAS/STAT*) *User's Guide, Version 6* (SAS Institute, Cary, NC, ed. 4, 1990), vol. 1. Linear discriminant analysis (LDA) is a classical linear statistical technique for classifying vectors of numbers (in this case, the Δ values) according to known examples, where the vectors are assumed to follow a multivariate normal distribution with known or (as in this case) estimated parameters. Thus, LDA can be considered a purely linear equivalent of the network. See, for example, D. J. Hand, *Discrimination and Classification* (Wiley, New York, 1981).
19. The McNemar test is a binomial calculation based on the discrepant predictions of the two methods that asks how likely it is that the difference in the number of incorrect predictions arose by chance [Q. NcNemar, *Psychometrika* **12**, 153 (1947)].
20. Standard techniques of cluster analysis on the 60-line screen patterns (with a Euclidean distance metric and average linkage clustering) supported evidence from the neural network that the category of DNA antimetabolites is functionally highly diverse.
21. As one additional example, calculations were done to assess predictiveness for each category as opposed to any other category. Given a single, overall optimum threshold, a network with nine hidden layer elements made an average of 3.5 mistakes per category out of a possible 141.

22. We thank J. S. Driscoll for help in identifying mechanisms of action; B. Bunow, B. A. Chabner, S. M. Sieber, and J. S. Driscoll for critical reading of the manuscript; and R. D. Everly and G. Ferruzza for technical assistance with the software.

15 May 1992; accepted 1 September 1992

Age and Duration of Weathering by ^{40}K-^{40}Ar and $^{40}Ar/^{39}Ar$ Analysis of Potassium-Manganese Oxides

Paulo M. Vasconcelos, Tim A. Becker, Paul R. Renne, George H. Brimhall

Supergene cryptomelane $[K_{1-2}(Mn^{3+}Mn^{4+})_8O_{16} \cdot xH_2O]$ samples from deeply weathered pegmatites in southeastern Brazil subjected to ^{40}K-^{40}Ar and $^{40}Ar/^{39}Ar$ analysis yielded ^{40}K-^{40}Ar dates ranging from 10.1 ± 0.5 to 5.6 ± 0.2 Ma (million years ago). Laser-probe $^{40}Ar/^{39}Ar$ step-heating of the two most disparate samples yielded plateau dates of 9.94 ± 0.05 and 5.59 ± 0.10 Ma, corresponding, within 2 σ, to the ^{40}K-^{40}Ar dates. The results imply that deep weathering profiles along the eastern Brazilian margin do not reflect present climatic conditions but are the result of a long-term process that was already advanced by the late Miocene. Weathering ages predate pulses of continental sedimentation along the eastern Brazilian margin and suggest that there was a time lag between weathering and erosion processes and sedimentation processes.

Rates of chemical interaction between rocks and the hydrosphere and atmosphere at the Earth's surface have only rarely been constrained by direct dating techniques (*1*). Radiocarbon residence times, uranium series dating (*2*), thermoluminescence techniques, and more recently ^{10}Be (*3*, *4*), ^{36}Cl (*5*, *6*), ^{26}Al (*3*), ^{3}He (*7*, *8*), and oxygen isotopes (*9*) have been used successfully in special cases to constrain weathering or exposure ages. The ages of many weathering surfaces in tectonically stable cratons, however, are beyond the useful limits of some of these techniques. Other techniques either are inapplicable because of the lack of datable overlying volcanic deposits (*9*) or are unreliable because they require assumptions about element immobility after incor-

P. M. Vasconcelos and G. H. Brimhall, Department of Geology and Geophysics, University of California, Berkeley, CA 94720.
T. A. Becker and P. R. Renne, Institute of Human Origins Geochronology Center, 2453 Ridge Road, Berkeley, CA 94709.

poration into the weathering profile (*3, 4*). Supergene alunites and jarosites formed by weathering have been dated directly by ^{40}K-^{40}Ar (*1*). Although the results are encouraging, the fine-grained nature of supergene alunite and jarosite (*1*), the relatively high solubility of alunite and jarosite in aqueous solutions, and the commonly intimate intergrowth of supergene alunite and jarosite with hypogene phases (*1*) restrict the applicability of these minerals as datable phases. Thus, a direct dating technique that can be broadly applied to products of hydrochemical weathering reactions is needed.

Modern laser-heating $^{40}Ar/^{39}Ar$ dating techniques have been successfully applied to the study of very small grains from igneous, metamorphic, and sedimentary rocks, as well as to the study of meteorites and lunar samples (*10*). The fine resolution possible with this method makes it uniquely suited to the study of complex mineral intergrowths present in the weathering environment. Ideally, a supergene mineral datable by the laser-heating $^{40}Ar/^{39}Ar$ method should (i) be widely distributed; (ii) be stable under most climatic environments; (iii) be easily separable, by physical methods, from hypogene phases; (iv) contain sufficient K; and (v) be retentive of Ar and K. Potassium-bearing manganese oxides, especially cryptomelane and hollandite, fulfill these requirements (*11*). In this report, we present the results of the application of ^{40}K-^{40}Ar and $^{40}Ar/^{39}Ar$ dating of K-Mn oxides to the study of weathering processes in southeastern Brazil.

A great variety of manganese oxides exist in nature (*12–14*); most are fine-grained. The most commonly known manganese oxide, pyrolusite (MnO_2), is thought to be the main component of soil manganese nodules and concretions, dendrites, and manganese coatings on weathered surfaces. Increasing application of fine-scale electron microscopy and spectroscopic techniques indicates that many of the manganese oxides in the weathering environment are actually complex manganese phases such as cryptomelane ($K_{1-2}Mn_8O_{16}{\cdot}xH_2O$), hollandite [$(Ba,K)_{1-2}Mn_8O_{16}{\cdot}xH_2O$], birnessite [$(Na,Ca,K)(Mg,Mn)Mn_6O_{14}{\cdot}3H_2O$], and todorokite [$(Na,Ca,K)(Mg,Mn^{2+})Mn_5O_{12}{\cdot}xH_2O$] (*12, 13, 15–17*).

We used ^{40}K-^{40}Ar and $^{40}Ar/^{39}Ar$ dating of authigenic cryptomelane to date the advance of weathering fronts in granite-pegmatitic bedrock in southeastern Brazil. The area of study, Divinos das Laranjeiras, Minas Gerais, Brazil (Fig. 1), is characterized by deeply weathered Precambrian and Proterozoic schists, gneisses, granites, and pegmatites surrounding rounded unweathered granitic-gneissic inselbergs (*18*).

Unweathered pegmatites contain coarse quartz, potassium feldspar, muscovite, biotite, tourmaline, beryl, spodumene, topaz, as well as phosphates, axinites, sulfides, and some carbonates, which commonly fill the large miarolitic cavities. These pegmatites are enriched in Mn, as indicated by the presence of Mn-bearing phosphates such as rockbridgeite, manganovariscite, frondelite, strunzite, and jahnsite (*19, 20*) and spessartite garnets. The reactive silicate, sulfide, carbonate, and phosphate minerals in pegmatites are readily weathered when exposed to acid oxidizing surface conditions. Weathering of feldspars and micas results in the formation of large amounts of kaolinite, whereas quartz remains unaltered. During weathering, the open miarolitic cavities become propitious loci for the precipitation of pure, euhedral, and coarse crystalline supergene phases. Supergene iron and manganese oxides form stalactitic and stalagmitic encrustations on weathering-resistant primary minerals such as quartz, beryl, and tourmaline and also occur as pseudomorphic replacement of primary phosphates, axinite feldspars, and garnet. We analyzed manganese oxides from eight different weathered pegmatites.

Scanning electron microscopy (SEM), electron microprobe analysis, x-ray diffraction, high-voltage electron microscopy (HVTEM), and analytical electron microscopy confirmed that the samples are monomineralic. Analysis of the samples by HVTEM and SEM indicated that single cryptomelane crystals are 10 to 20 μm long and <1 μm in diameter. We paid particular

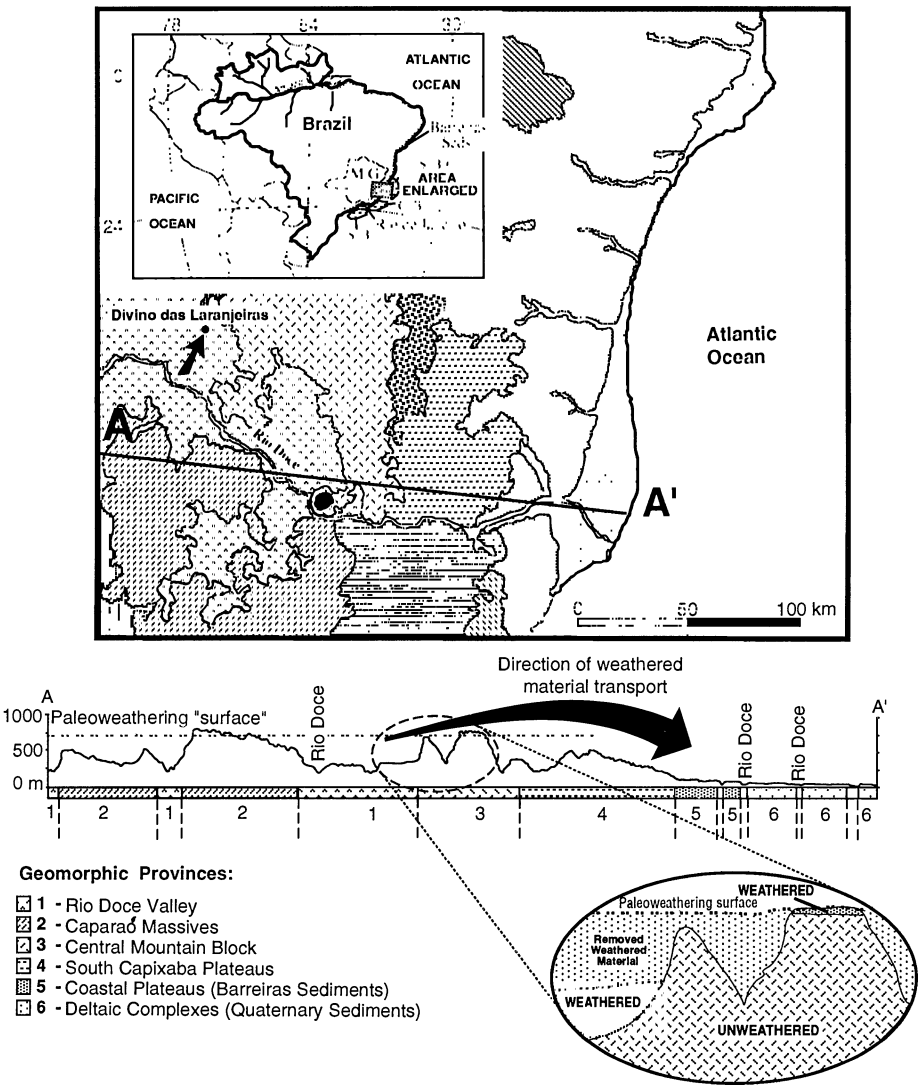

Fig. 1. Geologic map and cross section of the Rio Doce Valley area, southeastern Brazil, showing the location of deep weathering profiles and inselbergs in the interior and Tertiary and Quaternary sediments (South Capixaba plateaus, coastal plateaus, and deltaic complexes) along the coast. Sample location is indicated by a small arrow. The large arrow indicates the direction of sediment transport. The stippled pattern on the inset map indicates the location of Barreiras Group sediments deposited along the Brazilian coast. Minas Gerais State (MG), Campos Basin (C.B.), Espírito Santo Basin (E.S.B.), and Santos Basin (S.B.) are also shown on the inset map.

attention to the possibility of intergrown phases, particularly K-bearing phyllosilicates, that could affect the results obtained from ^{40}K-^{40}Ar and $^{40}Ar/^{39}Ar$ dating of the samples. One sample, PEG-05, was eliminated because it contained intergrown, partially weathered potassium feldspar and muscovite. The high K content and the monomineralic distribution of cryptomelane in the other specimens suggest that these samples are suitable for ^{40}K-^{40}Ar and $^{40}Ar/^{39}Ar$ dating. Selected samples were prepared for ^{40}K-^{40}Ar dating as in (*21*).

The ^{40}K-^{40}Ar ages for cryptomelane (Table 1) ranged from 10.1 ± 0.5 to 5.6 ± 0.2 Ma. Results for samples analyzed in duplicate (PEG-01 and PEG-02) were reproducible to within 2σ. A relatively small $\%^{40}Ar^*$ (percent of ^{40}Ar that is radiogenic) was obtained as compared to values typically obtained from igneous and metamorphic minerals. This difference probably reflects the large amount of intergranular pore space of supergene manganese oxides formed in contact with the atmospheric environment, which leads to high amounts of trapped atmospheric ^{40}Ar. In addition, a trapped atmospheric ^{40}Ar component associated with tunnel H_2O may contribute to the low $\%^{40}Ar^*$.

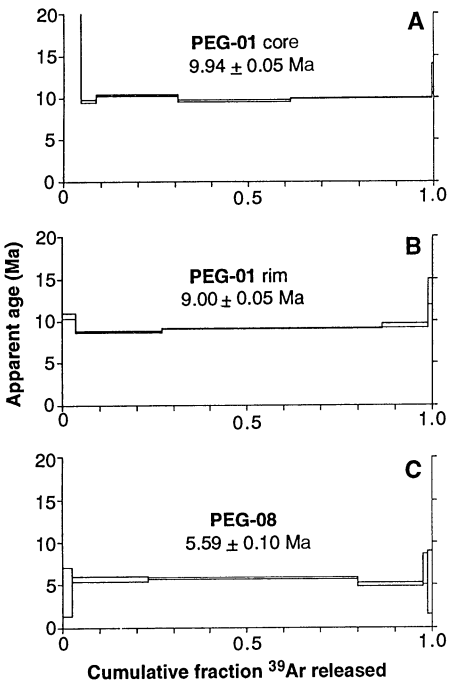

Fig. 2. Apparent age spectra, showing the apparent age as a function of the cumulative fraction of ^{39}Ar released, for samples PEG-01 core (3363-03) (**A**), PEG-01 rim (3363-06) (**B**), and PEG-08 (4309-02) (**C**). Sample PEG-01 indicates that weathering in southeastern Brazil was initiated at or sometime before 10 Ma. Sample PEG-08 dates from the last weathering event recorded in the southeastern Brazil profiles before climatic deterioration interrupted the weathering process.

PEG-01 and PEG-08, the oldest and the youngest samples, respectively, as indicated by ^{40}K-^{40}Ar analysis (Table 1), were selected for $^{40}Ar/^{39}Ar$ study. Sample PEG-01, which showed concentric growth bands, was sliced perpendicular to these botryoidal bands and sectioned into core and rim blocks weighing between 7 and 14 mg (*22*). Step-heating $^{40}Ar/^{39}Ar$ results for PEG-01 core (combined plateau age of 10.00 ± 0.05 Ma) and rim (plateau age of 9.00 ± 0.05 Ma) samples (Table 2 and Fig. 2, A and B) agree with the results of ^{40}K-^{40}Ar analysis and indicate that the rim was deposited 940,000 years after the core (*23*). The average growth rate was $6.4 \times 10^{-3} \pm 1.2 \times 10^{-3}$ mm per thousand years (1σ uncertainty). Regression of $^{39}Ar/^{40}Ar$ versus $^{36}Ar/^{40}Ar$ isotope correlation trends yielded results that are analytically indistinguishable from the plateau dates within 2σ errors, and initial $^{40}Ar/^{36}Ar$ values that are indistinguishable from the present atmospheric values of 295.5. Results for sample PEG-08 (Fig. 2C and Table 2) also agree with the ^{40}K-^{40}Ar (5.60 ± 0.20 Ma) and combined $^{40}Ar/^{39}Ar$ (5.59 ± 0.10 Ma) dates.

Potential problems in the interpretation of the ages include the following:

1) Loss of Ar or K from the manganese oxide structures due to diffusion or exchange with ground water. For our samples, the reproducible steps within a sample, yielding apparent age plateaus, strongly suggest that the system has behaved as a closed system and that Ar loss by slow diffusion or K exchange with weathering solutions does not pose problems.

2) Contamination of the supergene phases by intergrown hypogene phases or inherited protolith material. Extensive reflected and polarized light petrography, SEM and TEM investigation, and electron microprobe analysis along traverses that cross-cut whole thin sections indicate that the manganese oxides under study are monomineralic and do not contain intergrown hypogene phases.

3) Incorporation of ^{40}Ar (excess or inherited Ar) released from the primary minerals into the structure of supergene minerals. If this were the case, the isotope correlation regressions should yield $^{40}Ar/^{36}Ar$ intercepts significantly different from the present atmospheric value of 295.5 (*10*). This is not the case in any of the analyses presented.

4) Recoil of ^{39}Ar from the fine-grained acicular manganese oxide during neutron irradiation. A common problem in $^{40}Ar/^{39}Ar$ dating of fine-grained material is the loss or redistribution of nucleogenic ^{39}Ar by recoil (*24*). The problem arises from the displacement of ^{39}Ar by recoil (upon neutron production from ^{39}K) from the near-surface regions of crystals. The good agreement between ^{40}K-^{40}Ar and $^{40}Ar/^{39}Ar$ results in this study is clear and unequivocal evidence that recoil loss of ^{39}Ar from manganese oxides during neutron irradiation is not significant, a fact that we attribute to the high density of manganese oxides.

5) The presence of multiple generations of manganese oxides, with recurrent precipitation, dissolution, and reprecipitation. Manganese oxides in this study showed textural evidence of continuous growth and lacked textures indicating episodic dissolution and reprecipitation. The paragenetic textures identified indicate either that manganese oxides were stable after precipitation or that any episode of dissolution-reprecipitation totally erased previously precipitated phases. In either case, the apparent ages obtained reflect the last weathering episode that affected the manganese oxides we dated.

Our results suggest in this case that manganese oxides are suitable phases for ^{40}K-^{40}Ar and $^{40}Ar/^{39}Ar$ dating. We conclude that the results obtained in this investigation are valid precipitation ages of manganese oxides formed during weathering processes. Because the minerals analyzed come from different weathered pegma-

Table 1. Results of the ^{40}K-^{40}Ar analysis of supergene manganese oxides from Divino das Laranjeiras, MG, Brazil. K^+ analysis by atomic absorption.

Sample	K^+ (% by weight)	±1σ	Weight (g)	$^{40}Ar^*$ ($\times 10^{-11}$ mol/g)	$\%^{40}Ar^*$	Age (Ma)	±1σ (Ma)
PEG-01	4.66	0.15	0.27545	8.159	43.0	10.1	0.5
PEG-01	4.66	0.15	0.28021	7.524	28.1	9.3	0.5
PEG-01	4.66	0.15	0.54086	7.660	48.2	9.5	0.4
PEG-01	4.66	0.15	0.69993	8.116	30.8	10.0	0.5
PEG-02	4.29	0.12	0.50396	6.100	52.9	8.2	0.4
PEG-02	4.29	0.12	0.50396	6.022	52.4	8 1	0.3
PEG-03	4.42	0.12	0.50431	6.435	43.5	8.4	0.3
PEG-06	1.17	0.04	0.54768	1.608	19.3	7.9	0.7
PEG-07	2.23	0.06	0.58973	2.517	21.8	6.5	0.4
PEG-08	4.39	0.13	0.55349	4.291	42.4	5 6	0.2

Table 2. Results of $^{40}Ar/^{39}Ar$ dating for samples PEG-01 and PEG-08.

Lab No.	Laser (W)	$^{40}Ar^*/^{39}Ar$	$\%^{40}Ar^*$	Age (Ma)	± 1σ
		PEG-01 core			
3363-03	0.7	5.48	4.7	77.91	12.71
	1.0	0.66	35.0	9.63	0.20
	1.5	0.71	43.4	10.36	0.11
	2.0	0.67	48.2	9.71	0.09
	5.0	0.69	56.9	9.96	0.07
	6.0	0.84	8.5	12.23	1.77
3363-04	0.7	1.03	20.3	14.82	1.85
	1.0	0.74	13.9	10.71	1.31
	1.5	0.72	38.6	10.43	0.14
	2.0	0.74	9.5	10.68	0.72
	6.0	0.96	7.2	13.78	1.59
		PEG-01 rim			
3363-06	0.7	0.75	61.9	10.66	0.30
	1.0	0.62	44.3	8.76	0.09
	1.5	0.64	52.7	9.12	0.07
	2.0	0.66	23.8	9.42	0.25
	5.0	0.94	6.4	13.43	1.52
	6.0	0.82	3.1	11.60	2.52
3363-08	6.0	0.88	9.6	12.27	0.79
3363-09	0.7	1.00	7.3	13.77	1.15
	6.0	0.61	100.3	8.43	0.17
		PEG-08			
4309-01	0.3	0.50	3.7	4.12	1.33
	0.5	0.66	14.8	5.42	0.30
	8.0	0.82	15.4	6.71	2.40
4309-02	0.2	0.51	1.9	4.22	2.84
	0.3	0.69	14.4	5.71	0.31
	0.4	0.70	29.6	5.80	0.13
	0.5	0.62	25.4	5.09	0.21
	1.0	0.83	72.9	6.83	1.78
	8.0	0.64	3.1	5.29	3.70

tites, in distinct profiles, their relative depths cannot be used to monitor the progression of the weathering front through time. On the other hand, the presence of these supergene minerals at a depth of >20 m in the weathering profiles implies that deep weathering was already present in the eastern margin of Brazil by the late middle Miocene and that it continued until the late Miocene or early Pliocene.

Development of deep weathering in the late Miocene (10.1 ± 0.5 to 5.6 ± 0.2 Ma) is consistent with the presence of warm humid conditions in southeastern Brazil during this interval (*25–27*). Warm ocean water, as indicated by the biogeographic distribution of planktonic foraminifera at mid- to low-latitude South Atlantic sites during the late Miocene (*26*), led to high evaporation and precipitation rates (*28*). A variety of evidence consistent with this interpretation suggests that chemical weathering prevailed over mechanical weathering (*29*). For example, the tropical vegetation cover expanded (*29*), and rivers draining southeastern Brazil were poor in dissolved and suspended load, analogous to the tributaries of the Amazon River draining the Brazilian and Guiana shields today (*30*). As a result, carbonate sedimentation prevailed over terrigenous deposition on the marginal basins, for example, Campos (*29, 31*), Espírito Santo (*29, 31*), and Santos basins (*32*). Clastic deposition in the Espírito Santo Basin was controlled by the sediment input from the Rio Doce (Fig. 1), and upper Miocene deposits contain abundant kaolinite (*29, 33*). These conditions are consistent with well-drained humid tropical conditions in the interior (*30, 34*).

The interruption in the manganese oxide precipitation in weathering profiles at approximately 5.6 ± 0.2 Ma coincides with an observed transition from tropical humid to semi-arid to arid conditions in eastern Brazil (*29, 35*). The transition of a drier climate further inhibited large-scale dissolution of primary minerals and precipitation of supergene oxides. The early Pliocene in Brazil is defined by a sharp increase in continental sedimentation (*29, 35*) and a drop in sea level, as indicated by a hiatus in the Campos Basin stratigraphic record (*31*). Continental sediments were deposited along the Brazilian Atlantic margins from Rio de Janeiro to the mouth of the Amazon River (Fig. 1) (*29, 35*). The environment is believed to have been arid to semi-arid, with seasonal torrential rains (*29, 35*). The presence of abundant iron and aluminum oxide fragments in the detritus indicates that the source areas were deeply weathered, possibly lateritized, and extensively distributed throughout the Brazilian craton (*35*). The weathering history derived from the record of manganese oxide precipitation is consistent with the paleoclimatic history in southeastern Brazil.

REFERENCES AND NOTES

1. R. P. Ashley and M. L. Silberman, *Econ. Geol.* **71**, 904 (1976); C. N. Alpers and G. H. Brimhall, *ibid.* **100**, 1640 (1988); M. I. Bird, A. R. Chivas, I. McDougall, *Chem. Geol.* **80**, 133 (1990).
2. S. A. Short, R. T. Lowson, J. Ellis, D. M. Price, *Geochim. Cosmochim. Acta* **53**, 1379 (1989).
3. K. Nishiizumi, D. Lal, J. Klein, R. Middleton, J. R. Arnold, *Nature* **319**, 134 (1986); D. Lal, *Annu. Rev. Earth Planet. Sci.* **16**, 355 (1988).
4. M. J. Pavich, L. Brown, J. N. Valette-Silver, J. Klein, R. Middleton, *Geology* **13**, 39 (1985).
5. F. M. Phillips, B. D. Leavy, N. O. Jannik, D. Elmore, P. W. Kubik, *Science* **231**, 41 (1986).
6. F. M. Phillips *et al.*, *ibid.* **248**, 1529 (1990).
7. M. D. Kurz, *Geochim. Cosmochim. Acta* **50**, 2855 (1986).
8. T. E. Cerling, *Quat. Res.* **33**, 148 (1990).
9. M. I. Bird and A. R. Chivas, *Geochim. Cosmochim. Acta* **53**, 3239 (1989).
10. I. McDougall and T. M. Harrison, *Geochronology and Thermochronology by the $^{40}Ar/^{39}Ar$ Method* (Oxford Univ. Press, New York, 1988).
11. An advantage of the ^{40}K-^{40}Ar and $^{40}Ar/^{39}Ar$ methods is that they are independent of calibration horizons, because they depend only on the in situ decay of ^{40}K to ^{40}Ar. These techniques also have a wide age range of application, from a few tens of thousands of years to billions of years.
12. R. G. Burns and V. M. Burns, in *Marine Minerals*, P. H. Ribbe, Ed. (Mineralogical Society of America, Washington, DC, 1979), pp. 1–46.
13. R. M. Potter and G. R. Rossman, *Am. Mineral.* **64**, 1199 (1979).
14. Manganese commonly occurs in the II, III, and VI valence states in nature: Mn^{2+} is the most common cation in weathering and soil solutions, whereas Mn^{4+} is readily precipitated as relatively insoluble manganese oxides [D. A. Crerar, R. K. Cormick, H. L. Barnes, in *Geology and Geochemistry of Manganese*, I. M. Varentsov and G. Grasselly, Eds. (E. Scweizerbart'sche Verlagsbuchhandlung, Stuttgart, Germany, 1980), pp. 293–334]. Manganese mobility in the weathering environment is enhanced by acid-reducing conditions created by organic acids, which stabilize Mn^{2+} in the weathering solutions. Abundant vegetation and the organic acids generated by plant decay contribute to the mobility of Mn in the weathering environment [D. A. Crerar, R. K. Cormick, H. L. Barnes, *Acta Mineral. Petrogr. Szeged.* **20**, 217 (1972)].
15. M. Amouric, A. Baronnet, D. Nahon, P. Didier, *Clays Clay Miner.* **34**, 45 (1986).
16. R. Giovanoli, in *Geology and Geochemistry of Manganese*, I. M. Varentsov and G. Grasselly, Eds. (E. Schweizerbart'sche Verlagsbuchhandlung, Stuttgart, Germany, 1980), pp. 159–202.
17. The hollandite-type structure consists of Mn^{4+} (and minor Mn^{3+}, Fe^{3+}, Al^{3+}, and Si^{4+}), in octahedral coordination forming double chains where MnO octahedra share edges. Vertex-sharing double chains form large channels filled by the H_2O and A cations (Ba^{2+}, K^+, Pb^+, Na^+, Cu^{2+}, Sr^{2+}, Rb^{2+}) in eightfold coordination with oxygen atoms from the double chains. Large cations such as Ba^{2+} and K^+ occupying the A site give stability to the hollandite structure. Even though some of the hollandite group minerals have pronounced cation-exchange properties because of the low activation energy of cations in the A site, W. Sinclair, G. M. McLaughlin, and A. E. Ringwood [*Acta Crystallogr. Sect. B* **36**, 2913 (1980)] noticed that the channels in the hollandite structure contain narrow square-shaped bottlenecks, which decrease cation mobility along the tunnels. Restricted cation mobility in the tunnel structure has important implications for the Ar retentivity of hollandite-type minerals.
18. F. F. M. Almeida and Y. Hasui, *O Pré-Cambriano do Brasil* (Edgard Blucher Ltda, São Paulo, Brazil, 1984).
19. C. C. Farias, *Univ. Fed. Pernambuco-Dep. Eng. Minas-Estud. Pesq.* **6/7**, 81 (1984).
20. J. Cassedanne and J. Cassedanne, *An. Acad. Bras. Ciênc.* **54**, 165 (1982).
21. P. M. Vasconcelos, T. A. Becker, P. R. Renne, G. H. Brimhall, in preparation.
22. The blocks were packed in ultrapure aluminum containers, and the containers were stacked in a ten-level column. Fragments from the same PEG-08 split used in ^{40}K-^{40}Ar determinations were packed in the same way. A similar column containing Fish Canyon sanidine (27.84 Ma) as the fast neutron fluence monitor was also prepared. The columns were wrapped together in aluminum foil and irradiated in the Omega West Nuclear Reactor at Los Alamos National Laboratory for 7 hours.
23. The samples were step-heated with an Ar-ion continuous laser using a defocused beam. Analytical procedures and equipment are described in the following: A. L. Deino and R. Potts, *J. Geophys. Res.* **95**, 8453 (1990); A. L. Deino, L. Tauxe, M. Monaghan, R. Drake, *J. Geol.* **98**, 567 (1990). Data corrected for mass discrimination, nucleogenic interferences, and atmospheric contamination were used to calculate apparent ages for each degassing step.
24. G. Turner and P. H. Cadogan, *Geochim. Cosmochim. Acta* **2**, 1601 (1974); J. C. Huneke and S. P. Smith, *Geochim. Cosmochim. Acta* (Suppl.) **7**, 1987 (1976); T. M. Harrison, *Isotope Geosci.* **1**, 319 (1983); C. H. Lo and T. C. Onstott, *Geochim. Cosmochim. Acta* **53**, 2697 (1989).
25. P. R. Supko and K. Perch-Nielsen, *Init. Rep. Deep Sea Drilling Proj.* **39**, 1099 (1977).

26. R. Thunell and P. Belyea, *Micropaleontology* **28** (no. 4), 381 (1982).
27. S. M. Savin, *Annu. Rev. Earth Planet. Sci.* **5**, 319 (1977); S. M. Savin *et al.*, *Geol. Soc. Am. Mem.* **163**, 49 (1985).
28. L. A. Frakes, *Climates Throughout Geologic Time* (Elsevier, Amsterdam, 1979).
29. S. Petri and V. J. Fúlfaro, *Geologia do Brasil* 1-631 (Universidade de São Paulo, São Paulo, Brazil, 1983); M. R. Silva *et al.*, in *Projeto RADAM Folha SE.24 Rio Doce* (Instituto Brasileiro Geografia Estatística, Rio de Janeiro, 1987), pp. 23–172.
30. R. J. Gibbs, *Geol. Soc. Am. Bull.* **78**, 1203 (1967); J. D. Milliman and R. H. Meade, *J. Geol.* **91**, 1 (1983); R. H. Meade, T. Dunne, J. E. Richey, U. de M. Santos, E. Salati, *Science* **228**, 488 (1985); R. F. Stallard and J. M. Edmond, *J. Geophys. Res.* **88**, 9671 (1983); *ibid.* **92**, 8293 (1987).
31. A. Bertels, R. L. Milward de Azevedo, A. C. F. Mesquita, W. d. S. Abreu, *B. Geoci. PETROBRAS* **3**, 175 (1989); R. L. Antunes, N. T. Sonoki, M. Carminatti, *Rev. Bras. Geoci.* **18**, 283 (1988).
32. P. C. Soares and P. M. B. Landim, *An. Acad. Bras. Ciênc.* **47**, 343 (1975).
33. U. Melo, C. P. Summerhayes, J. Ellis, *Contrib. Sedimentol.* **4**, 78 (1975).
34. H. Chamley, *Clay Sedimentology* (Springer-Verlag, Berlin, 1989).
35. L. C. King, *Rev. Bras. Geogr.* **18**, 3 (1956); J. J. Bigarella, *Geol. Soc. Am. Spec. Pap.* **84**, 433 (1965); *An. Acad. Bras. Ciênc.* **47**, 385 (1975); J. J. Bigarella, D. Andrade-Lima, P. J. Riehs, *ibid.*, p. 411; K. Beurlen, *Bol. Soc. Bras. Geol.* **16**, 43 (1967); J. M. Mabesoone, A. C. E. Silva, K. Beurlen, *Rev. Bras. Geoci.* **2**, 173 (1972); K. Suguio, J. C. Bidegain, N. A. Mörner, *ibid.* **16**, 171 (1986); M. V. Rabelo, *Geociências* **5**, 79 (1986).
36. We acknowledge the support of the Brazilian Research Council (CNPq) to P.M.V. (grant 200392/88-3/GL) and the National Science Foundation to G.H.B. (grants EAR 8804136 and 9018747). This project has benefited from discussions with W. Dietrich, H. Helgeson, G. Sposito, and H.-R. Wenk and from comments by G. B. Dalrymple and an anonymous reviewer. We also thank the *garimpeiro* Orílio Vaz de Aguilar from Divino das Laranjeiras for help with the collection of manganese oxide samples from the pegmatites.

20 April 1992; accepted 27 July 1992

Some Anthropological Aspects of the Prehistoric Tyrolean Ice Man

Horst Seidler, Wolfram Bernhard, Maria Teschler-Nicola, Werner Platzer, Dieter zur Nedden, Rainer Henn, Andreas Oberhauser, Thorstein Sjøvold

The corpse of a Late Neolithic individual found in a glacier in Oetztal is unusual because of the intact nature of all body parts that resulted from the characteristics of its mummification process and its protected geographical position with regard to glacier flow. Anthropological data indicate that the man was 25 to 40 years old, was between 156 and 160 centimeters in stature, had a cranial capacity of between 1500 and 1560 cubic centimeters, and likely died of exhaustion.

In the autumn of 1991 a mummified corpse (known also as the "man from Hauslabjoch" or "the Similaun man") was found after having been released by glacier ice in the Tyrolean Oetztaler Alps. After a number of attempts by amateurs to remove the corpse it was recovered in a professional way by forensic experts from the University of Innsbruck, Austria. The original position of the corpse could therefore not be determined (*1*). Thereafter the corpse was stored and preserved in the Anatomy Department at the University of Innsbruck. The corpse is now under simulated glacial conditions at a relative humidity of 96 to 98% and a temperature of −6°C. Radiocarbon dating of the corpse conducted independently in Oxford and in Zurich have shown that the corpse is between 5200 and 5300 years old (*2*). In this report, we present anthropological results on the find that may be of general interest for further discussions and investigations. The morphometric and morphological investigations have required painstaking efforts in conservation. It is not possible to remove the mummy from its refrigerator for longer than 30 min because of the risk of deterioration that thawing would cause on structural features of the tissue. Considering the time necessary for preparation and maintenance, hardly 15 min remained for each examination. Our first examinations of morphological details therefore have been carried out only to a small degree on the corpse itself. For more extensive examinations (for example, analysis of metric data or the description of cranial sutures) three-dimensional reconstructions were made (*3*). For this we used two lines of approach: One was the measurement and examination of rotated computer tomography (CT) sectional pictures. The other involved plastic reconstruction of the skull (Fig. 1).

Because of their special interest for physical anthropologists, we have included a selection of some metric characters of the skull (Table 1). These measurements demonstrate that the morphological characteristics of the "man in ice" are well within the measurement ranges of Late Neolithic and Bronze Age populations as have been described in the literature (*4*, *5*). Note the hyperorthognate facial form expressed in the facial and alveolar angles of the profile. The estimation of cranial capacity according to different estimates of multiple analysis regressions was between 1500 and 1560 cm^3 (*6*, *7*) (Table 2).

The measured stature of the "man in ice" also ranges within the known variation of Neolithic populations as have been described from Italy and Switzerland (*8*). During one of the earlier attempts to recover the mummy, a pneumatic drill was used to partially extract the corpse out of ice. Severe damage occurred in the left pelvic region, and the caput femoris was set free. From the isolated caput femoris the physiologic length of the femur was measured and used for the estimation of the body stature. This measurement of the extremities and several sections of the rump of the corpse with a measuring tape showed that the bodily stature was between 156 and 160 cm. The estimates arrived at by regression (*9*) correspond to the stature that was arrived at by direct measurement (158 cm).

An estimation of the age at death is based on the degree of wear of the front teeth. The remarkably strong degree of abrasion indicates an age of between 35 and 40 years. Sometimes, however, an extreme-

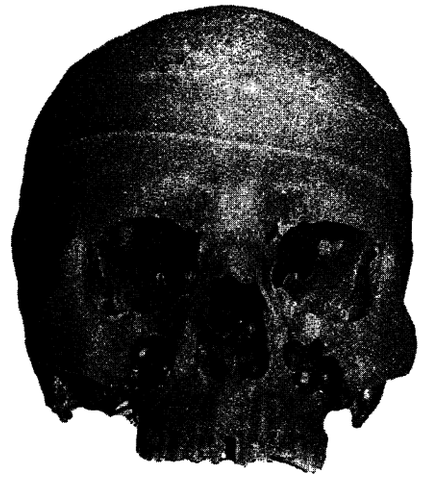

Fig. 1. Three-dimensional reconstruction of the skull as described in the text. The right orbita is slightly displaced; the medial trema is easily recognizable.

H. Seidler, Institut für Humanbiologie der Universität Wien, Athanstrasse 14, A-1091 Wien, Austria.
W. Bernhard, Institut für Anthropologie der Universität Mainz, Saarstrasse 21, DW-6500 Mainz, Germany.
M. Teschler-Nicola, Anthropologische Abteilung, Naturhistorisches Museum Wien, Burgring 7, A-1010 Wien, Austria.
W. Platzer, Institut für Anatomie der Universität Innsbruck, Müllerstrasse 59, A-6010 Innsbruck, Austria.
D. zur Nedden and A. Oberhauser, Abteilung für Röntgendiagnostik und Computertomographie der Universitätsklinik Innsbruck, Anichstrasse 35, A-6020 Innsbruck, Austria.
R. Henn, Institut für Gerichtliche Medizin der Universität Innsbruck, Müllerstrasse 44/III; A-6020 Innsbruck, Austria.
T. Sjøvold, Osteological Research Laboratory, University of Stockholm, S-171 71 Solna, Sweden.